Front. Earth Sci. 2021, 15(3): 705–718
https://doi.org/10.1007/s11707-020-0843-z

REVIEW ARTICLE

Prediction of natural fracture in shale oil reservoir based on *R/S* analysis and conventional logs

Haoran XU[1,2], Wei JU (✉)[1,2], Xiaobing NIU[3,4], Shengbin FENG[4], Yuan YOU[4], Hui YANG[1,2], Sijia LIU[5], Wenbo LUAN[2]

1 Key Laboratory of Coalbed Methane Resources and Reservoir Formation Process (Ministry of Education) China University of Mining and Technology, Xuzhou 221008, China
2 School of Resources and Geosciences, China University of Mining and Technology, Xuzhou 221116, China
3 School of Geosciences, China University of Petroleum (East China), Qingdao 266580, China
4 Institute of Exploration and Development, PetroChina Changqing Oilfield Company, Xi'an 710018, China
5 School of Computer Science and Technology, China University of Mining and Technology, Xuzhou 221116, China

Abstract Investigation into natural fractures is extremely important for the exploration and development of low-permeability reservoirs. Previous studies have proven that abundant oil resources are present in the Upper Triassic Yanchang Formation Chang 7 oil-bearing layer of the Ordos Basin, which are accumulated in typical low-permeability shale reservoirs. Natural fractures are important storage spaces and flow pathways for shale oil. In this study, characteristics of natural fractures in the Chang 7 oil-bearing layer are first analyzed. The results indicate that most fractures are shear fractures in the Heshui region, which are characterized by high-angle, unfilled, and ENE-WSW-trending strike. Subsequently, natural fracture distributions in the Yanchang Formation Chang 7 oil-bearing layer of the study area are predicted based on the *R*/*S* analysis approach. Logs of AC, CAL, ILD, LL8, and DEN are selected and used for fracture prediction in this study, and the $R(n)/S(n)$ curves of each log are calculated. The quadratic derivatives are calculated to identify the concave points in the $R(n)/S(n)$ curve, indicating the location where natural fracture develops. Considering the difference in sensitivity of each log to natural fracture, gray prediction analysis is used to construct a new parameter, fracture prediction indicator *K*, to quantitatively predict fracture development. In addition, fracture development among different wells is compared. The results show that parameter *K* responds well to fracture development. Some minor errors may probably be caused by the heterogeneity of the reservoir, limitation of core range and fracture size, dip angle, filling minerals, etc.

Received June 21, 2020; accepted October 15, 2020

E-mail: wju@cumt.edu.cn

Keywords natural fracture prediction, shale oil reservoir, *R*/*S* analysis, Chang 7 oil-bearing layer, Ordos Basin

1 Introduction

Low-permeability reservoirs refer to those whose air permeability is less than 50×10^{-3} μm^2, and when the air permeability of a reservoir is less than 10×10^{-3} μm^2, it may be called an ultralow-permeability reservoir (Zeng and Li, 2009). Due to the compactness and brittle lithology of low-permeability reservoirs, natural fractures are easily generated under the influence of intense diagenesis and later tectonic effects (Zeng and Li, 2009). Low-permeability reservoirs play an important role in continental sedimentary basins (Zeng and Liu, 2010). If natural fractures are developed in this type of reservoir, physical properties may be changed, and the reservoir quality will be greatly improved. Natural fractures can provide effective storage spaces for oil and gas accumulation and connect existing matrix pores in reservoirs, resulting in the increase of permeability (Zeng et al., 2016; Lyu et al., 2017; Shi et al., 2020; Zeng and Liu, 2010). In addition, natural fractures may affect the selection of drilling and completion methods, hydraulic fracturing and oil and gas development (Zeng and Liu, 2010; Zeng et al., 2016; Lyu et al., 2017; Shi et al., 2020). Previous studies have indicated that there are abundant shale oil resources in the Chang 7 oil-bearing layer of the Upper Triassic Yanchang Formation in the Ordos Basin (Yang et al., 2016). Its air permeability is less than 0.3×10^{-3} μm^2, hence it is a typical ultralow-permeability reservoir. Natural fractures in the reservoir are relatively developed, which serve as major pathways for fluid flow (Zeng and Li, 2009; Zeng

et al., 2010; Zhao and Hou, 2017). Thus, it is of great significance to study the distribution of natural fractures in the Chang 7 shale reservoir for effective exploration and development.

There are many methods to identify natural fractures in reservoirs, including analysis based on cores, imaging log data, etc. (Lai et al., 2018; Lyu et al., 2017). However, these methods are commonly expensive, and many wells lack core and imaging log data. Hence, when facing data shortage, it is difficult to obtain valuable information (Tokhmechi et al., 2009; Zazoun, 2013; Lyu et al., 2016; Su et al., 2017). In addition, many other methods can be used to study natural fractures, among which, conventional logs are inexpensive and easy to obtain. However, due to the weak fracture response of the conventional log, one can hardly accurately identify natural fractures based on a single conventional log to natural fracture. It is necessary to use some algorithms and more logs to improve the accuracy. In recent years, many scholars have made advancements in this field. For example, Tokhmechi et al. (2009) applied petro-physical logs to identify natural fractures by combining wavelet, classification, and data-fusion techniques. Based on an adaptive neuro-fuzzy inference system, Ja'fari et al. (2012) established the fracture density estimation model based on conventional logs. Zazoun (2013) used an artificial neural network (ANN) to predict natural fracture density through the conventional log curve. Ge et al. (2014) used kernel principal component analysis (KPCA) and multifractal detrended fluctuation analysis (KPCA-MFDFA) to predict the development degree of natural fractures. Lyu et al. (2016) and Aghli et al. (2020) have identified fractures by enhancing natural fracture responses of conventional logs through various log curves. Zhang et al. (2011) combined wavelet transforms with conventional log differential curves for fracture identification. Fractal theory has also been proven to be able to analyze reservoir characteristics and determine the development location of fractures (Pang and North, 1996; Xiao et al., 2019; Li et al., 2020).

In this paper, with a case study of the Heshui region in the Ordos Basin, we first analyze the characteristics of natural fractures in the Yanchang Formation Chang 7 shale reservoir based on limit cores and imaging logs. Then, the *R*/*S* analysis method is used to identify natural fractures and predict the development and distribution of fractures, which are tested by statistical data measured from the cores. The results are expected to provide more geological references for shale oil production in the study area.

2 Geologic setting

The Ordos Basin, located between the Siberian Craton and South China Craton, is a N-S-trending basin in the west of the North China Craton, covering an area of 2.69×10^5 km^2 (Hou et al., 2010; Zhao and Hou, 2017). It can be divided into six sub-structural units, namely, the Yimeng uplift, Weibei uplift, western margin thrust belt, Tianhuan depression, Yishan slope and Jinxi flexure belt. The Ordos Basin has stable internal structural activity, but its edge deformation is strong, which forms many folds and faults (Liu et al., 2009; Ju et al., 2020a). The study area, the Heshui region, is located in the southwestern Ordos Basin (Fig. 1). The depositional period of the Yanchang Formation Chang 7 oil-bearing layer was the prosperity period of basin development, when the lake was the largest (Yang et al., 2016; Fu et al., 2018; Ju et al., 2020b). Hence, during this period, the basin deposited a set of river-delta-lacustrine strata (Yang et al., 2016; Fig. 2). A set of fresh water organic-rich shale was deposited, which is the important oil source system in the Ordos Basin (Ju et al., 2015; Wu et al., 2015; Yang et al., 2017), hence shale oil resources are mainly enriched in the Chang 7 oil-bearing layer. Further, the Yanchang Formation can be divided into 10 oil-bearing layers: Chang 1 to Chang 10, from top to bottom. The Chang 7 oil-bearing layer can be further divided into three sub-oil-bearing layers, namely, Chang 7_1, Chang 7_2 and Chang 7_3 sub-oil-bearing layers, from top to bottom (Yang et al., 2016). Natural fractures in the Chang 7 reservoir are relatively developed, providing migration channels for shale oil and enhancing the conductivity of reservoir. The development of natural fractures may also increase the reservoir space and provide conditions for shale oil accumulation (Yang et al., 2017).

3 Fracture characteristics

Based on the core and imaging log data, the characteristics of natural fracture in the Yanchang Formation Chang 7 oil-bearing layer are analyzed (Figs. 3–5). Natural fractures can be divided into three types according to the fracture dip angle: high-angle fractures (70°–90°), oblique fractures (30°–70°), and low-angle fractures (less than 30°) (Zeng et al., 2009).

In this study, a total of 45 fractures are discovered from 180.7 m core data in 5 wells in the Heshui region (Fig. 4). These fractures are mainly high-angle fractures (86.7%). Low-angle fractures and oblique fractures mainly appear in mudstones, while most high-angle fractures are in sandstones. Most of these fractures were unfilled, and the filling minerals in those few natural fractures are mainly calcite.

In total, 56 natural fractures are discovered from imaging logs in the study area (Figs. 3 and 5). Among those fractures, high-angle fractures account for 94.6%. The others are oblique and low-angle fractures. The strikes of the identified fractures in the study area are mainly ENE-WSW-trending (Fig. 6).

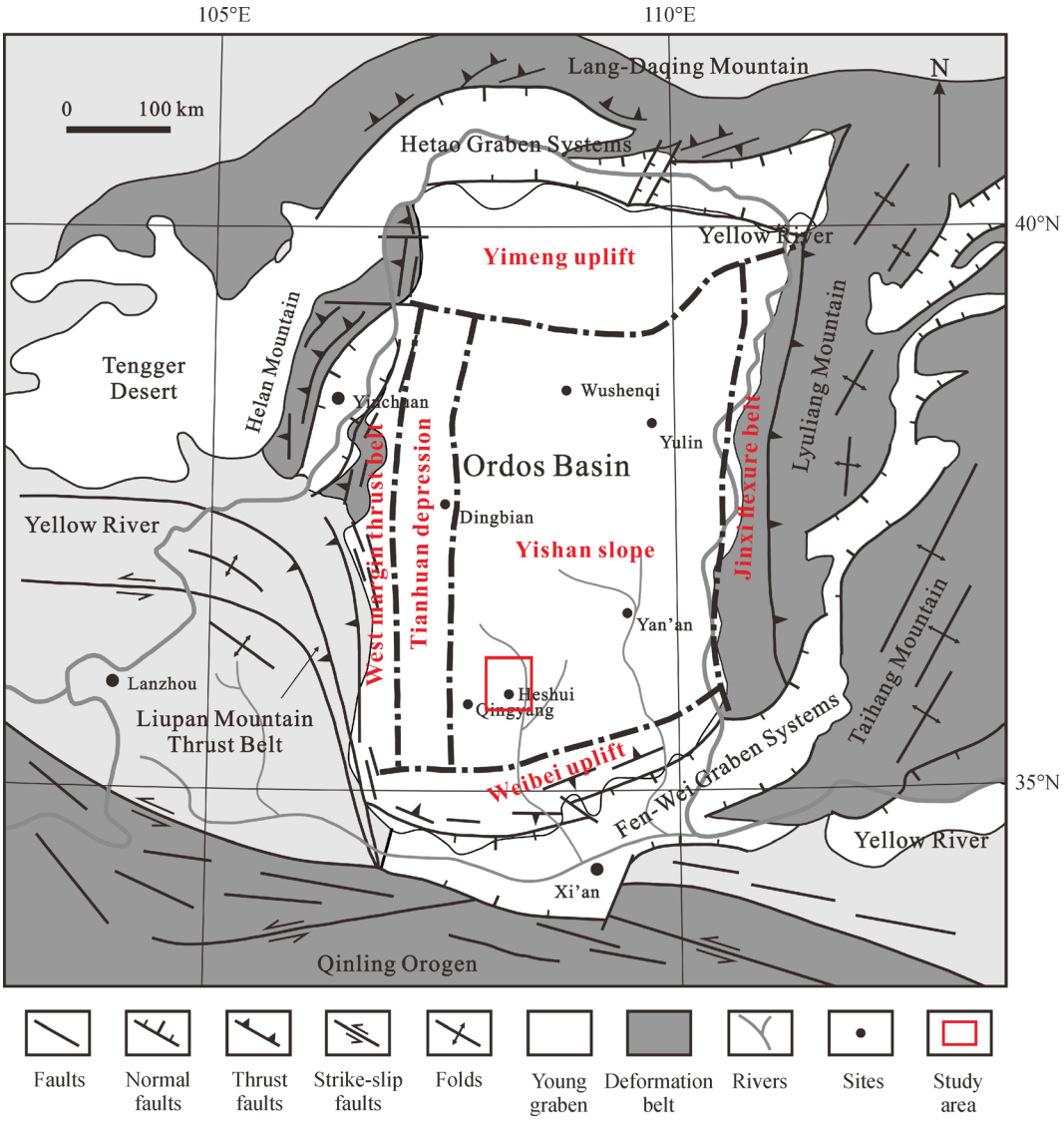

Fig. 1 Regional geological background of the Ordos Basin (Darby and Ritts, 2002; Ritts et al., 2004).

4 Theory and method

Using conventional log data to identify fractures has the advantages of easy access and low cost. However, it is difficult to identify fractures by simply using original logging data. To better identify the development of fractures from the conventional log, the combination of log data and various mathematical algorithms is usually used to identify fractures. Previous studies have performed considerable research and put forward a variety of data processing methods, such as wavelet decomposition, classification and data fusion (Tokhmechi et al., 2009), adaptive neuro-fuzzy inference system (Ja'fari et al., 2012), artificial neural network (Zazoun, 2013), wavelet transforms (Zhang et al., 2011), kernel principal component analysis and multifractal detrended fluctuation analysis (Ge et al., 2014), and enhancement of the fracture response and elimination of the non-fracture response (Lyu et al., 2016). In addition, the *R*/*S* analysis method is used as an effective fractal method to analyze reservoir fracture characteristics (Pang and North, 1996; Xiao et al., 2019; Li et al., 2020).

The *R*/*S* analysis method, which is also called rescaled-range analysis, was originally developed by Hurst in 1951 to study the long-term variations of the Nile River (Hurst, 1951). Later, this method was proven to be an effective method for analyzing one-dimensional fractal variables, and gradually, it was applied to analyze the long-term memory effect and memory period of various natural phenomena (Pang and North 1996; Miranda and Andrade, 1999; Rangarajan and Sant, 2004; Beretta et al., 2005; Zhao et al., 2011; Xiao et al., 2019; Li et al., 2020). In this method, *R* represents the range, which is the difference between maximum and minimum cumulative deviation. *S*

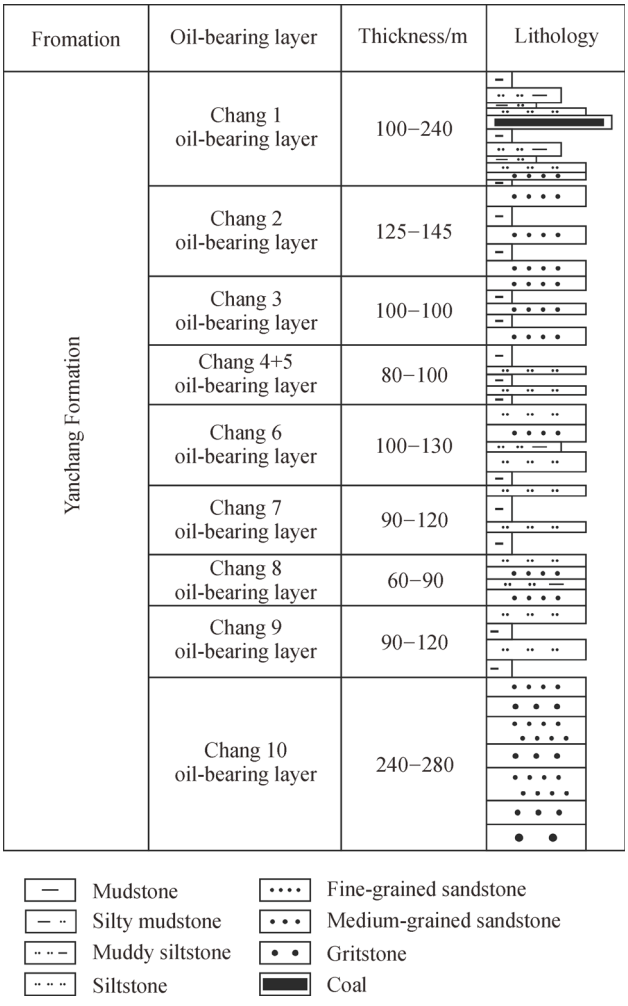

Fig. 2 Stratigraphic column of the Yanchang Formation in the Ordos Basin (Zeng and Li, 2009).

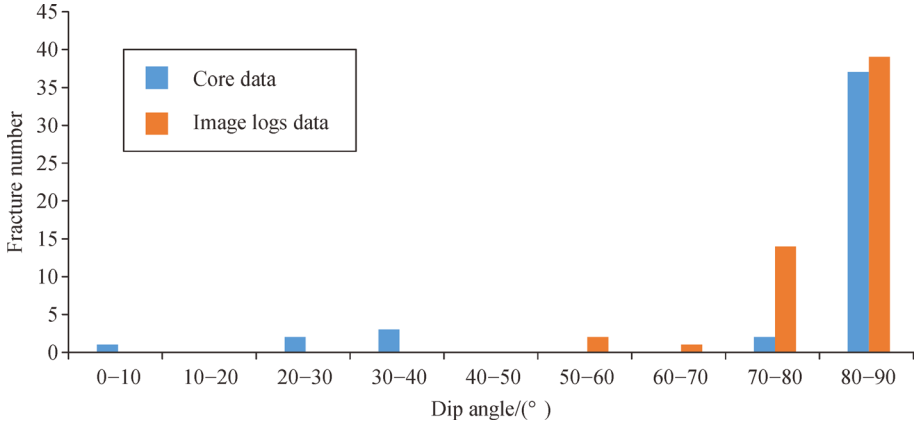

Fig. 3 Frequency histogram of the types of fractures obtained from the imaging logs date and core date.

is the standard deviation, that is, the square root of variance, which represents the average trend of time series. *R/S* represents a time series of fluctuations (Xiao et al., 2019; Li et al., 2020). The specific calculation process is as follows (Hou, 1994; Pang and North, 1996):

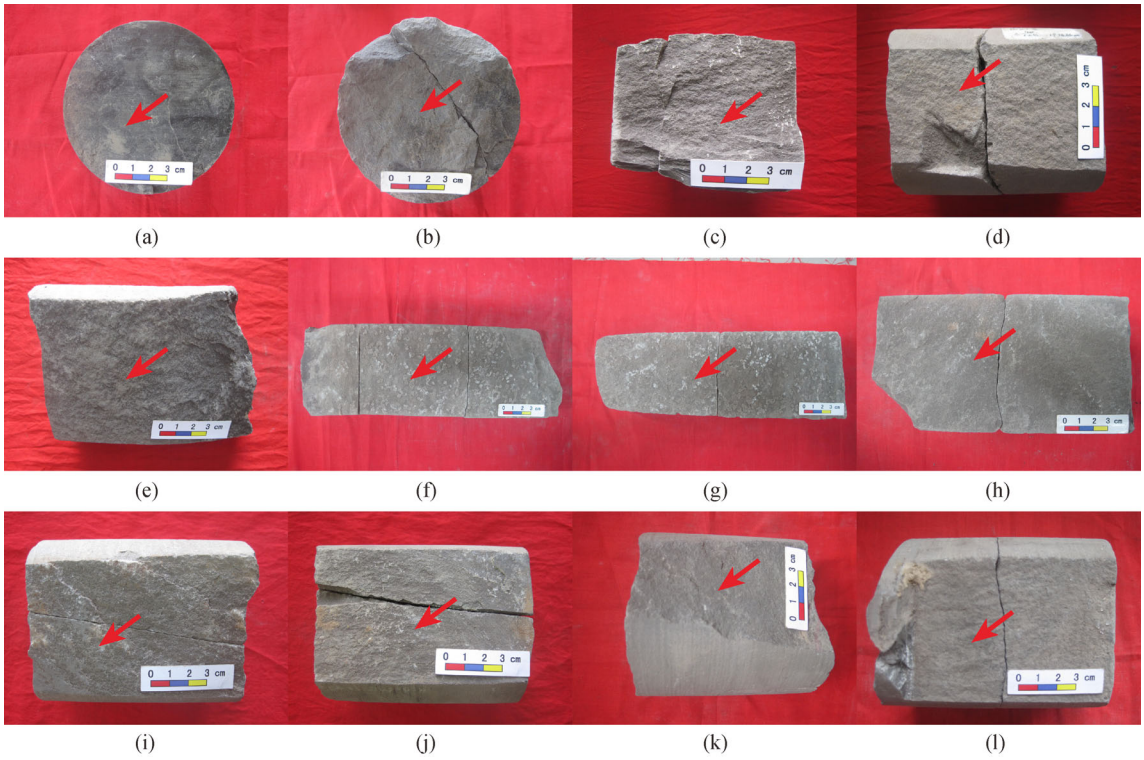

Fig. 4 Fracture characteristics from the cores, where the red arrows indicate natural fracture.
(a) low-angle fracture, Z15, 1991.45–1991.52 m; (b) low-angle fracture, Z15, 2010.4–2010.5 m; (c) high-angle fracture, Z87, 1972.2–1972.26 m; (d) high-angle fracture, Z87, 1976.58–1976.7 m; (e) high-angle fracture, Z87, 1987.49–1987.62 m; (f) high-angle fracture, filled with calcite, Z186, 1718.92–1719.21 m; (g) high-angle fracture, filled with calcite, Z186, 1719.46–1719.74 m; (h) high-angle fracture, Z186, 1725.57–1726.75 m; (i) high-angle fracture, Z200, 1866.76–1866.93 m; (j) high-angle fracture, Z200, 1867.01–1867.15 m; (k) high-angle fracture, Z230, 1755.45–1755.56 m; (l) high-angle fracture, Z230, 1755.61–1755.75 m.

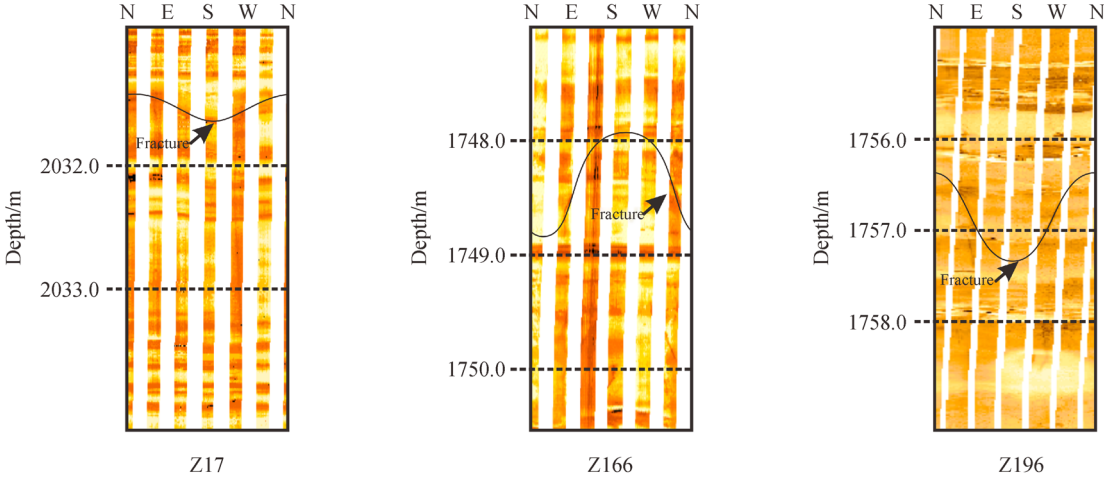

Fig. 5 Fracture characteristics in the imaging logs.

$$R(n) = \max_{0<\mu\leqslant n}\left\{\sum_{i=1}^{\mu} Z(i) - \frac{\mu}{n}\sum_{j=1}^{\mu} Z(j)\right\} - \min_{0<\mu\leqslant n}\left\{\sum_{i=1}^{\mu} Z(i) - \frac{\mu}{n}\sum_{j=1}^{\mu} Z(j)\right\}, \quad (1)$$

$$S(n) = \sqrt{\frac{1}{n}\sum_{i=1}^{\mu} Z^2(i) - \left[\frac{1}{n}\sum_{i=1}^{\mu} Z(j)\right]^2}. \quad (2)$$

The relationship between $R(n)/S(n)$ and n is:

$$\frac{R(n)}{S(n)}=\frac{\max\limits_{0<\mu\leqslant n}\left\{\sum_{i=1}^{\mu}Z(i)-\frac{\mu}{n}\sum_{j=1}^{\mu}Z(j)\right\}-\min\limits_{0<\mu\leqslant n}\left\{\sum_{i=1}^{\mu}Z(i)-\frac{\mu}{n}\sum_{j=1}^{\mu}Z(j)\right\}}{\sqrt{\frac{1}{n}\sum_{i=1}^{\mu}Z^2(i)-\left[\frac{1}{n}\sum_{i=1}^{\mu}Z(j)\right]^2}},\tag{3}$$

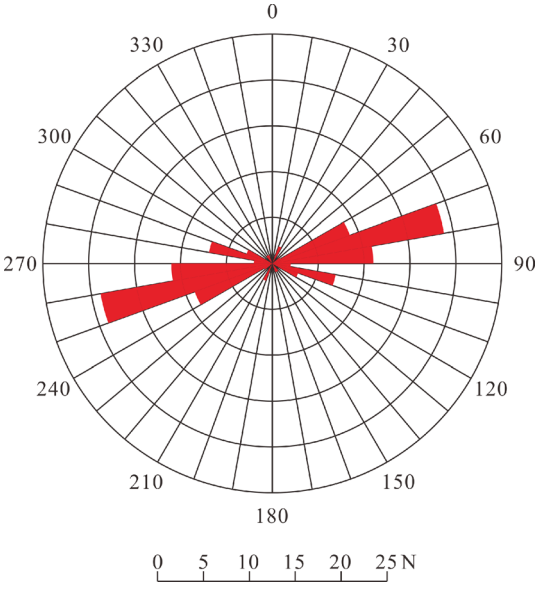

Fig. 6 Rose diagram of the strikes of natural fractures in the study area.

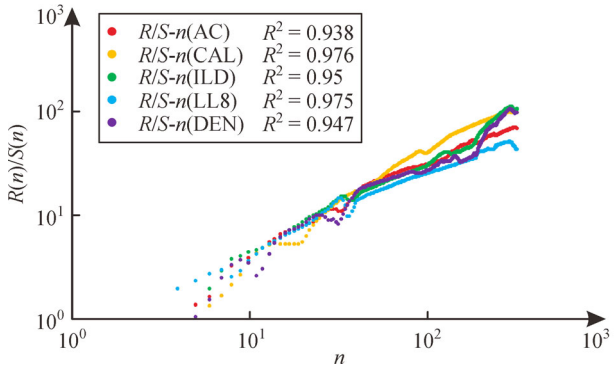

Fig. 7 Double logarithm curve of $R(n)/S(n)$ and n of AC, CAL, ILD, LL8 and DEN in Well Z200.

where Z is a one-dimensional time series, which is a vertical sequence of reservoir parameters and equivalent to the value of the conventional log; n is the total number of log sampling points in the layer to be analyzed; u is the number of samples and gradually increases from 0 to n; and i and j are variables of the number of sampling points, respectively.

For each n greater than 2, a corresponding $R(n)/S(n)$ value can be calculated. Then, the calculated $R(n)/S(n)$ and n are made into a double logarithmic scatter diagram. If there is a linear relationship between each lg$n$ and lg[$R(n)/S(n)$], Z has fractal characteristics. The fractal dimension D of Z represents the complexity of the one-dimensional variation of the sequence, which can be calculated by $D = 2H$. The parameter H, which is called the Hurst index, is the slope of the logarithmic curve (Hou, 1994; Hu, 2000; Liu et al., 2008). Hence, for parameter sequence Z, fractal dimension D indicates the heterogeneity of the vertical variation of reservoir. The existence of fractures will increase the heterogeneity of reservoir; that is, D will increase, which will decrease the slope of $R(n)/S(n)$ and the deviation of its linear relationship. As a result, when other factors are considered homogeneous, the concave section of the $R(n)/S(n)$ curve can be considered the fracture developing section.

Because of multiple solutions of the conventional log, using a single conventional log may lead to inaccurate fracture identification due to the influence of non-fracture information. Conventional logs generally include acoustic log (AC), density log (DEN), compensated neutron log (CNL), deep induction log(ILD), medium induction log (ILM), laterolog 8 (LL8), caliper log (CAL), gamma-ray log(GR) and spontaneous potential log (SP). However, ILM log data in some target beds are absent, and fracture responses of SP, GR and CNL are not obvious in this study. Therefore, 5 log curves are used to comprehensively identify fractures, namely, AC, CAL, ILD, LL8 and DEN.

$$Y=\frac{X-X_{\min}}{X_{\max}-X_{\min}}.\tag{4}$$

The normalized curves are calculated according to Eq. (4), and the $R(n)/S(n)$ values of each curve are obtained. Then, the calculation result is taken as a double logarithm, and the corresponding $R(n)/S(n)$ curve is drawn. The calculation result is shown in Fig. 7. Each curve has a good linear relationship, and the correlation is above 0.9, which indicates that each curve has a high fractal feature. The concave part of the curve indicates the development of natural fractures, but the accuracy of this artificial concave part identification is poor because it may easily cause error. Thus, the quadratic derivatives of the $R(n)/S(n)$ curve of each curve is obtained according to the previous methods (Xiao et al., 2019; Li et al., 2020). As is known, the quadratic derivative can reflect the concavity and convexity of the curve. If the quadratic derivative is greater than zero, the original function is concave, which indicates the position of fracture development. In contrast, the function curve is convex, which means natural fracture is

not developed.

It is impossible to directly derive the curve because $R(n)/S(n)$ is discrete data; hence, only approximate values can be obtained. According to the definition of the derivative, the derivative formula is as follows:

$$f'(x_0) = \lim_{\Delta x \to 0} \frac{\Delta y}{\Delta x} = \lim_{h \to 0} \frac{f(x_0 + h) - f(x_0 - h)}{2h}, \quad (5)$$

$$f''(x_0) = \lim_{\Delta x \to 0} f'(x_0) = \lim_{h \to 0} \frac{f(x_0 + h) + f(x_0 - h) - 2f(x_0)}{h^2}. \quad (6)$$

If T is the value of $R(n)/S(n)$, h is 1, and K is the quadratic derivative of $R(n)/S(n)$, then K is approximated to:

$$K = f''(x_0) \approx T_{n+1} + T_{n-1} - 2T_n. \quad (7)$$

The approximate quadratic derivative of the R/S curve of Well Z200 is calculated by Eq. (7). The final calculation results are shown in Fig. 8. The results show that the positive value of the quadratic derivative corresponds to the concave section of each curve, which proves the reliability of this method.

In this study, five log curves were used to predict fractures. The results are shown in Fig. 9. Each curve can reflect the degree of fracture development, but their sensitivity to natural fracture is different, hence the weight of each curve needs to be considered. In this study, we use gray prediction analysis to calculate the weight of selected five curves.

In the following, it is necessary to determine the fracture density to check the reliability of K. Here, the fracture density is calculated from the ratio between the total length of fractures and the area of the measured core. To match the log data with the discrete fracture density, the target formation is segmented according to the distribution of natural fractures. The presence of natural fracture will affect the K value around it, and the divided fracture

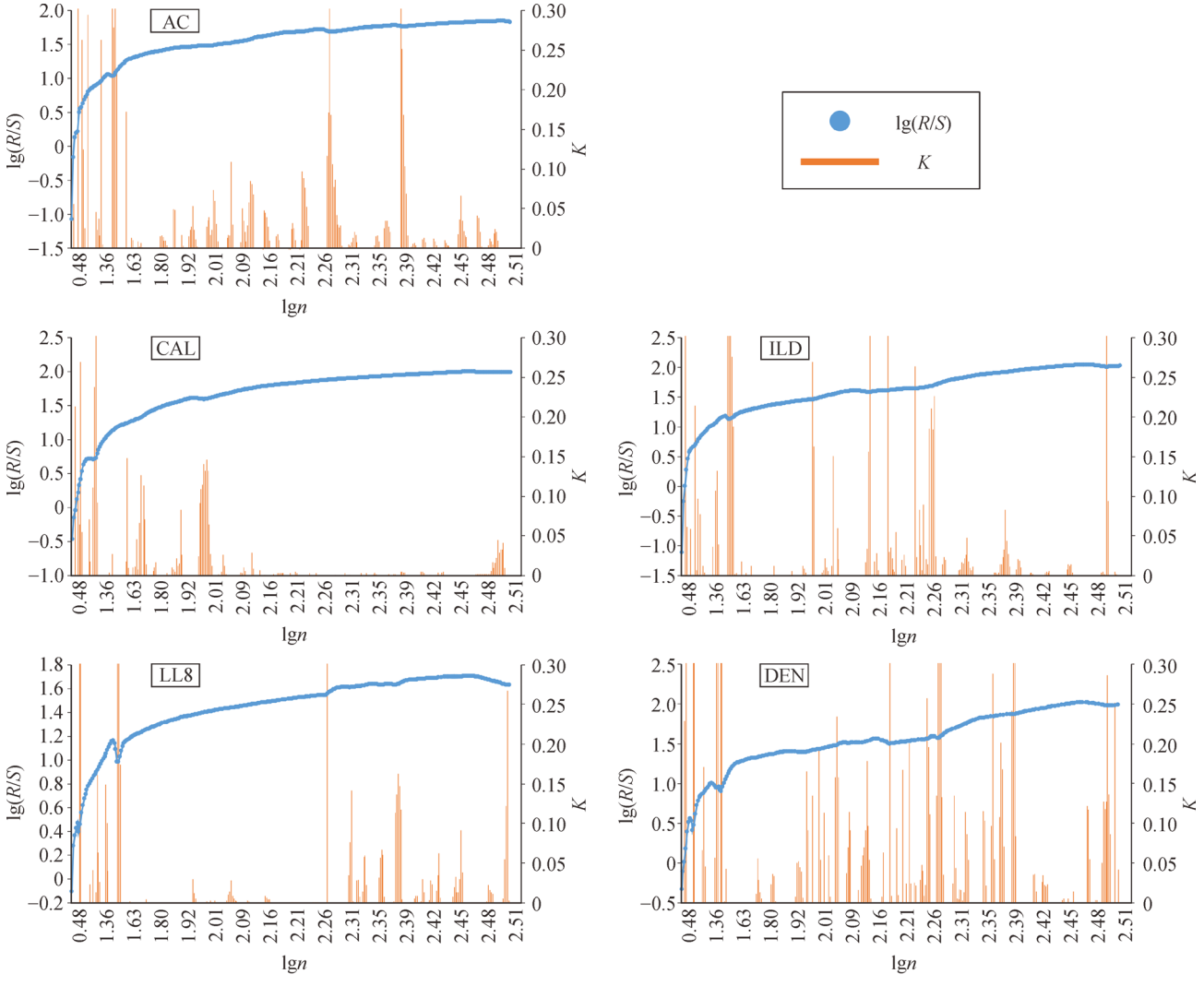

Fig. 8 The relationship between the concave sections of the $R(n)/S(n)$ curve and their quadratic derivative.

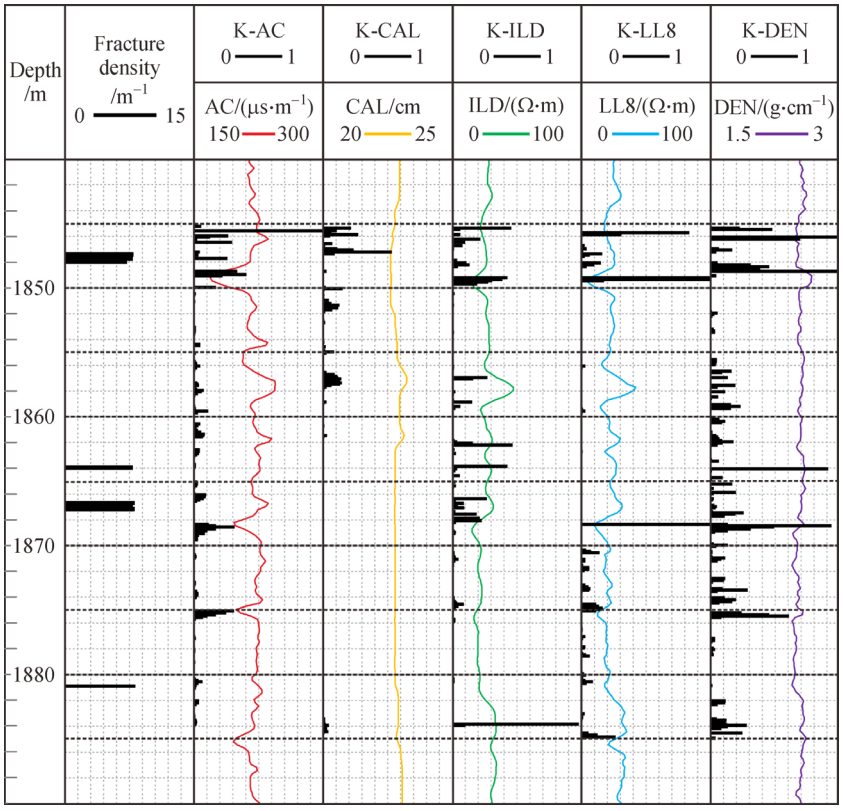

Fig. 9 Log curves of the fracture zones in the core data and *R*/*S* calculation results of each log in Well Z200. The fracture density is the surface density observed in the core. *K* is the strength of the fracture response. The black dotted line is the dividing line of the gray correlation analysis.

segment should contain high-*K* part as long as possible. In addition, the shortest possible non-fracture section should be included. After many attempts, the best length for the fracture segment division is 5 m (the gray solid line in Fig. 9). The average *K* in each fracture segment is calculated according to the divided layers. The basic data to calculate the weight of *K* value by the gray correlation analysis are shown in Table 1.

To explore the correlation between *K* of each log curve and fracture density, the fracture density is taken as the primary sequences and *K* is used as the subsequence. Then, the basic data are standardized based on Eq. (8) (Table 2):

$$Y = \frac{X}{X_{\max}}. \tag{8}$$

Then, gray relation coefficient ξ and gray relational grade r can be obtained based on Eqs. (9)–(11):

$$\xi = \frac{\Delta\min + \rho\Delta\max}{\Delta(i,j) + \rho\Delta\max}, \tag{9}$$

$$\Delta(i,j) = |Yi,j - Y'ij|, \tag{10}$$

Table 1 The basic data of the gray correlation analysis

Depth	Fracture	K-AC	K-CAL	K-ILD	K-LL8	K-DEN
1845–1850m	1.043	0.105	0.046	0.074	0.144	0.146
1850–1855m	0.000	0.005	0.020	0.001	0.000	0.005
1855–1860m	0.000	0.017	0.027	0.019	0.003	0.039
1860–1865m	0.141	0.016	0.002	0.033	0.001	0.051
1865–1870m	0.729	0.040	0.000	0.037	0.029	0.085
1870–1875m	0.000	0.006	0.000	0.011	0.032	0.040
1875–1880m	0.000	0.025	0.001	0.002	0.010	0.041
1880–1885m	0.196	0.010	0.007	0.028	0.018	0.039

Table 2 The standardized data of the gray correlation analysis

Depth	Fracture	K-AC	K-CAL	K-ILD	K-LL8	K-DEN
1845–1850m	1.000	1.000	1.000	1.000	1.000	1.000
1850–1855m	0.000	0.048	0.435	0.014	0.000	0.034
1855–1860m	0.000	0.162	0.587	0.257	0.021	0.267
1860–1865m	0.135	0.152	0.043	0.446	0.007	0.349
1865–1870m	0.699	0.381	0.000	0.500	0.201	0.582
1870–1875m	0.000	0.057	0.000	0.149	0.222	0.274
1875–1880m	0.000	0.238	0.022	0.027	0.069	0.281
1880–1885m	0.188	0.095	0.152	0.378	0.125	0.267

$$r = \frac{1}{n}\sum_{i=1}^{n} \xi(i), \tag{11}$$

where $Y'(i)$ is the value of the primary sequences; $Y(i, j)$ is a series of subsequence corresponding to the parent sequence; Δmax and Δmin are the maximum and minimum values of all $\Delta(i, j)$, respectively; ρ is the resolution coefficient, usually taken as 0.5 (Zhao et al., 2003); and n is the length of the sequence, that is, the number of evaluation indicators. The calculation results are shown in Table 3.

In addition, r represents the correlation degree between sub-factors and the parent factor. The effect is much greater when the parameter r is closer to 1. Therefore, the formula of this weight value is as follows (Eq. (12)):

$$\alpha = r / \sum_{i=1}^{n} r(i). \tag{12}$$

Thus, the weight of each curve is obtained as shown in Table 4.

The formula for natural fracture prediction is as follows (Eq. (13)):

$$K = 0.208 \times K_{\mathrm{AC}} + 0.192 \times K_{\mathrm{CAL}} + 0.198 \times K_{\mathrm{ILD}} + 0.211 \times K_{\mathrm{LL8}} + 0.191 \times K_{\mathrm{DEN}},$$

where K is the strength of the fracture response. Layers with higher K values indicate that fractures are more likely to develop.

5 Results and discussion

5.1 Results

The weighted result is shown in Fig. 10. The core data are consistent with the calculated K value as shown in Fig. 10, and parameter K appears high around the location where natural fractures develop. The above model is applied to the prediction of natural fractures in other wells, and the comparison between prediction results and actual situation is shown in Fig. 11. The predicted K value has a strong

Table 3 The gray relation coefficient and gray relational grade

	Depth	K_{AC}	K_{CAL}	K_{ILD}	K_{LL8}	K_{DEN}
ξ	1845–1850m	1.000	1.000	1.000	1.000	1.000
	1850–1855m	1.136	2.244	1.039	1.000	1.098
	1855–1860m	1.463	2.680	1.735	1.060	1.764
	1860–1865m	1.049	1.262	1.889	1.367	1.613
	1865–1870m	1.910	3.000	1.569	2.424	1.334
	1870–1875m	1.164	1.000	1.425	1.636	1.784
	1875–1880m	1.681	1.062	1.077	1.199	1.804
	1880–1885m	1.265	1.102	1.545	1.180	1.227
r		0.786	0.724	0.748	0.798	0.722

Table 4 Weight value of each conventional logs

Logging parameter	AC	CAL	ILD	LL8	DEN	Sum
r	0.786	0.724	0.748	0.798	0.722	3.777
Weight (a)	0.208	0.192	0.198	0.211	0.191	

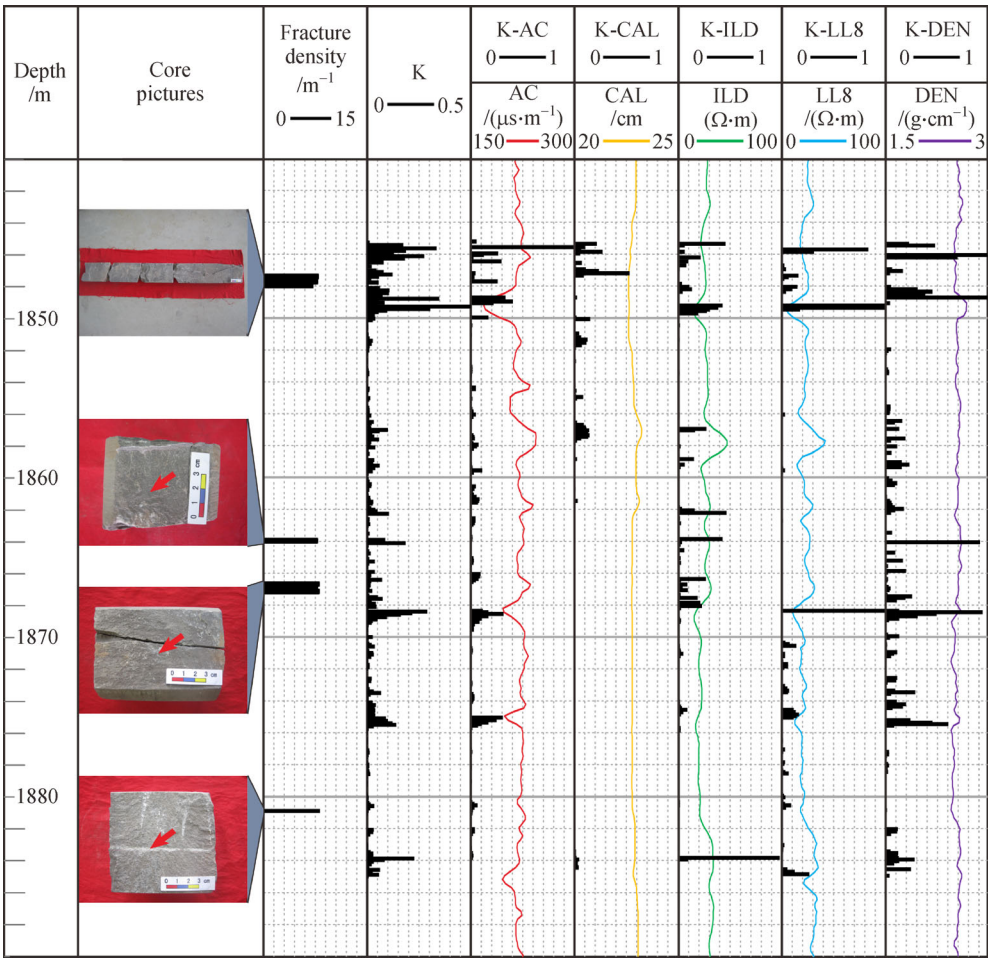

Fig. 10 Comparison of natural fracture zones in the core data and fracture zones recognized by the R/S analysis method in Well Z200.

fracture response in the fracture development layers. Hence, the results prove that the *R*/*S* analysis may accurately identify natural fractures.

5.2 Error analysis

The predicted results are generally consistent with those of the core data, but there are some errors. Responses in layers with high fracture density may be weaker than those with low fracture density in the same well. In addition, some layers where no fractures are found in the core have been predicted with high fracture response. That is, the calculated parameter *K* can perfectly identify natural fractures, but the development degree may have errors due to the following points.

One of the possible reasons is that some other factors in addition to natural fractures affect the prediction results. As previously mentioned, the *R*/*S* curve predicts fractures by identifying the reservoir heterogeneity. When the reservoir heterogeneity is enhanced (such as by dramatic changes in lithology or structure), the *R*/*S* curve will exhibit concave points, which will eventually lead to a wrong prediction. In this case, we will mistakenly think that there is a fracture at this location. For example, in Well Z186, natural fractures are mainly found in a core with a depth of 1718–1726 m, while the calculated results show that there are also high *K* values shallower than 1710 m and deeper than 1730 m. Based on investigations from the core data, interbedded sandstones and mudstones, many plant fossils, carbonaceous particles, and sulfur minerals are found at approximately 1703 m, 1707 m, and 1730 m, respectively (Fig. 12). These factors change the lithology, which makes the reservoir become heterogeneous; hence, the calculated results show differences in these locations. The effect caused by changes in lithology is also found in Well Z15. Although natural fractures are developed in the cores of 1990 m and 2010 m, the *K* value at 1990 m is obviously higher than that at 2010 m. According to the observations from the core data, flowing structure and sulfur are found near the depth of 1990 m (Fig. 12).

Another reason is that the drilled borehole does not cut across natural fracture. The extension range of a natural fracture is the range exposed by the core, and the absence of fracture in the core does not indicate that the adjacent

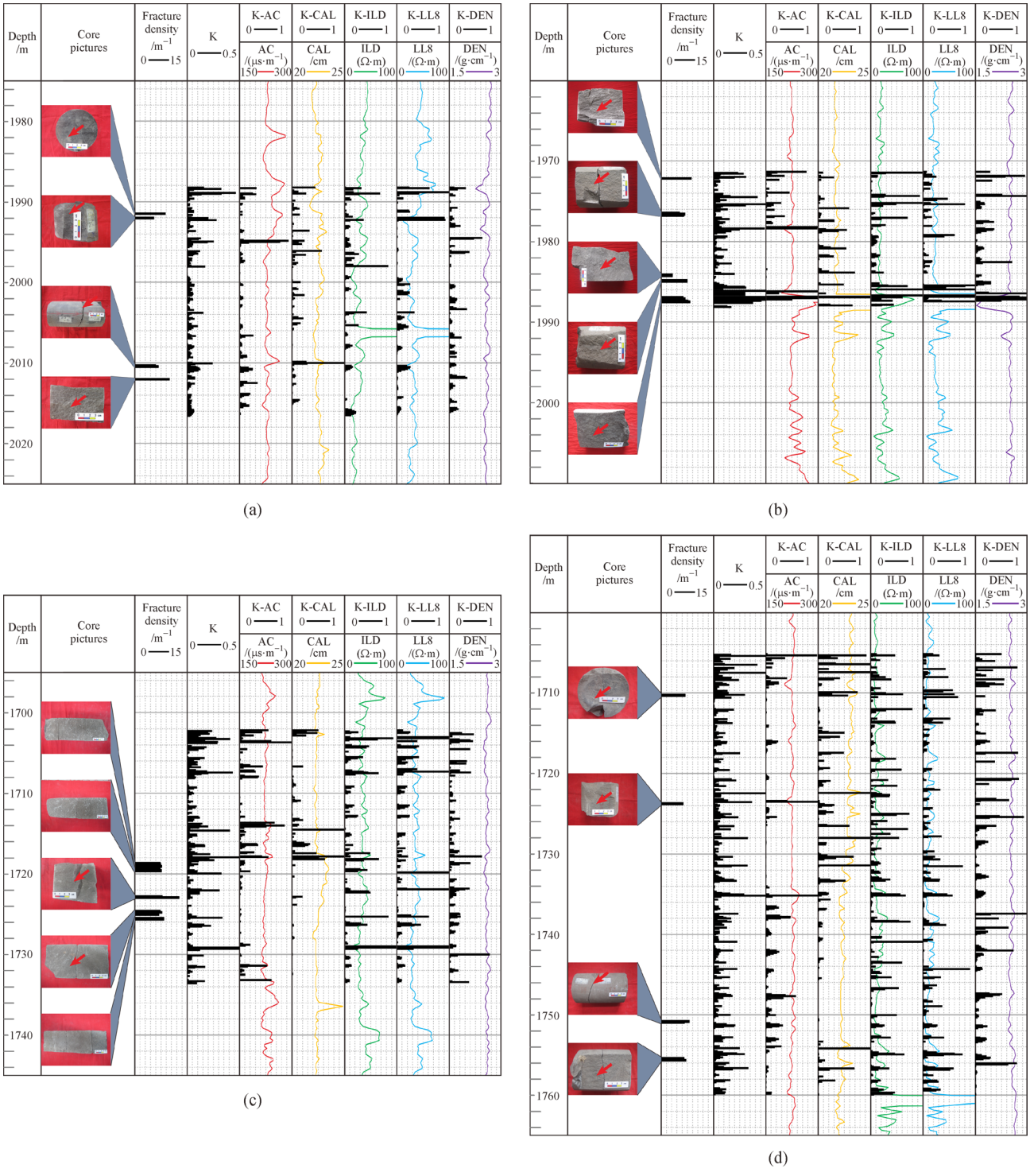

Fig. 11 Comparison of natural fracture zones in the core data and fracture zones recognized by the *R*/*S* analysis method in Wells (a) Z15, (b) Z87, (c) Z186 and (d) Z230.

rock is not fractured (Lyu et al., 2016). The core can only reveal the limit geological information, and it cannot detect the part that is not drilled. Therefore, we cannot absolutely determine that there must be no fractures around the core if no fractures are found in the core. However, the conventional log has a wider detection range, which can detect natural fractures around the drill, which are not found in the core. For the Chang 7 member of the Yanchang Formation in the study area, high-angle fracture represents the main type. Compared with the low-angle fractures, the high-angle fractures have a relatively small transverse expansion area due to the larger inclination

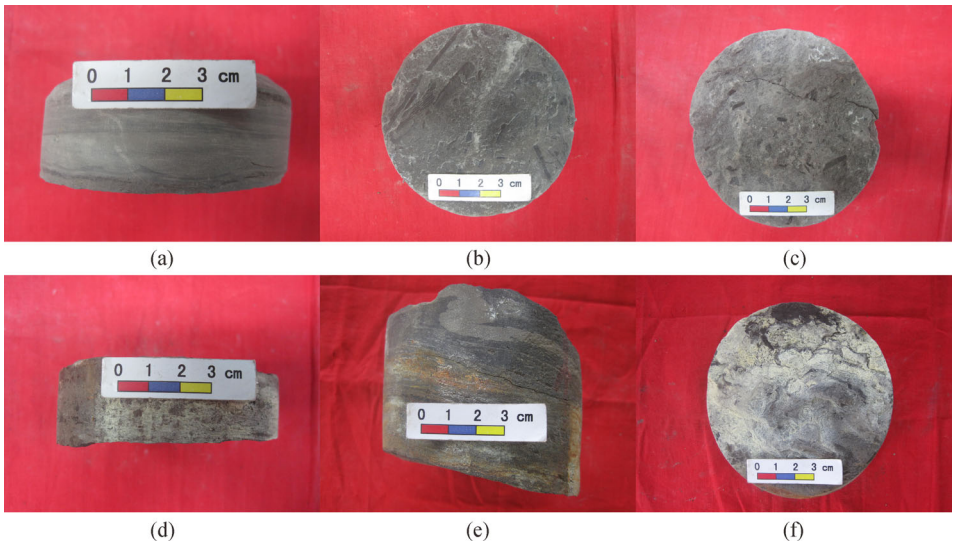

Fig. 12 The factors that influence the errors found in the rock core. (a) interbedded sandstones and mudstones, Z186,1703.5 m; (b) plant fossils, Z186, 1707.45 m; (c) carbonaceous particles, Z186,1731.5 m; (d) sulfur, Z186, 1732.87 m; (e) flowing structure, Z15, 1988.05 m; (f) sulfur, Z15, 1991.15 m.

angle. Hence, they have a lower probability to be revealed by drilling, which will make no fracture found in the core data, but the actual *K* value calculated from the logging data indicates that natural fracture is developed at this position. On the other hand, the drilled-through fractures are often only part of the whole fracture. There may still be an extension of fractures around the borehole, but we do not know how much of it has not been exposed. If two fractures of different sizes are drilled, but the larger fractures are less exposed, we will have a wrong view on the scale of fractures. The conventional logging has a larger detection range than core; hence, it can better identify the scale of fractures. Therefore, a low-fracture-density section in the core has a stronger fracture response than a high-fracture-density section.

In addition, the size of natural fractures will affect the accuracy of identification. Some intervals may develop micro-fractures, which are too small to be recognized in the core, and there are no records of micro-fractures in the core data. However, the existence of these micro-fractures will affect the identification of the conventional log: they make the log curve exhibit a fracture response to this interval, which results in the high calculated *K* value. This condition also causes a strong fracture response in the low-fracture-density section and non-fracture section. The existence of fillings in natural fractures can affect the fracture response. When fillings occur in a fracture, the fracture response will be weakened. The dip angle of fracture also affects the identification of fractures. The acoustic wave is more difficult to propagate through low-angle fractures. Hence, high-angle fractures will produce a weak fracture response.

The fracture prediction results among different wells are compared. The *K* values calculated for all wells are averaged, and the results are shown in Fig. 13. According

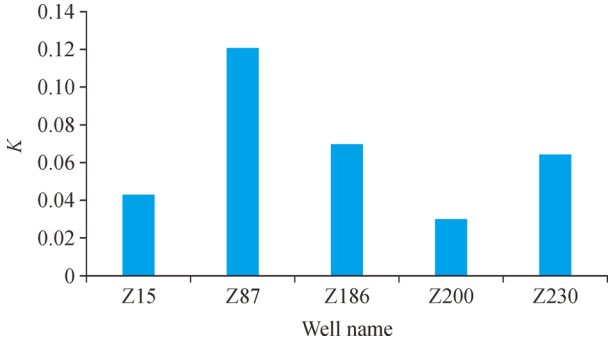

Fig. 13 Comparison of the average *K* values among different wells.

to the results, the *K* value in Well Z87 is 0.121 (the highest in all wells), which indicates that natural fractures in Well Z87 should be the most developed. By comparing core data, it is found that Well Z87 develops natural fractures with the highest density. The second is Well Z186, its *K* value is 0.07. The previous analysis indicates that the lithological and structural factors in Well Z186 affect the calculated *K* value, which makes the *K* value of Well Z186 higher than its actual value. The calculated *K* value of Well Z230 (0.064) is close to that of Well Z186. However, from the core data, the fracture density of Well Z230 is obviously lower than that of Well Z186. In addition, there are low-angle fractures in Well Z230, and the peak *K* value is not as steep as that in other wells. Therefore, it is speculated that fractures may develop around Well Z230. The *K* values of Well Z15 and Well Z200 were 0.043 and 0.03, respectively. A few fractures are developed in Well Z15, hence the *K* value is low. However, Well Z200 has lower *K* value, but more fractures are developed. Through the *K* value of conventional log curves, *K-CAL* has a weak

response to the area with depth more than 1860 m; thus, the finally calculated total *K* value is lower.

6 Conclusions

According to the core data and imaging log interpretation, vertical fractures are dominant within the reservoir of the Chang 7 member of the Yanchang Formation in the Heshui area, while other types of fractures are rare. Most of natural fractures were unfilled, and a few were filled with calcite. The strikes of the observed fractures are concentrated in the ENE-WSW directions.

The *R*/*S* analysis method can identify fractures by the conventional log. The double logarithmic curves of $R(n)/S(n)$ and n indicate that the Chang 7 Formation of the research area has better fractal characteristics. The concave point of the curve indicates the existence of natural fractures, but the artificial identification of the concave point is prone to large errors. The positive value of the quadratic derivative can identify the concave position in the $R(n)/S(n)$ curve.

Five kinds of conventional log are selected to identify natural fractures of the Chang 7 reservoir in the study area. Based on Well Z200, the weight value of each curve is obtained by gray prediction analysis. According to the weight value, the fracture prediction formula is obtained, and the calculated result has better fracture response. However, some errors remain, which can be inferred as follows: 1) the reservoir heterogeneity may interfere with the prediction results; 2) there are cracks around the core; and 3) the size, dip angle and cement of fracture affect the prediction results.

Compared with the prediction of different wells, natural fractures in Well Z87 are the most developed, followed by Well Z186, Well Z230, Well Z15, and Well Z200. Well Z186 may be influenced by lithological and structural factors, and there may be fractures around Well Z230. Natural fractures are less developed in Well Z15. The low total K value of Well Z200 may be due to the weak CAL response of this well.

Acknowledgements The authors would like to thank the anonymous reviewers for offering their constructive suggestions and comments, which have improved this manuscript in many aspects. The financial supports are from the National Natural Science Foundation of China (Grant Nos. 41702130 and 41971335), Natural Science Foundation of Jiangsu Province, China (BK20201349), and Priority Academic Program Development of Jiangsu Higher Education Institutions (PAPD).

References

Aghli G, Moussavi-Harami R, Tokhmechi B (2020). Integration of sonic and resistivity conventional logs for identification of fracture parameters in the carbonate reservoirs (a case study, Carbonate Asmari Formation, Zagros Basin, SW Iran). J Petrol Sci Eng, 186: 106728

Beretta A, Roman H E, Raicich F, Crisciani F (2005). Long-time correlations of sealevel and local atmospheric pressure fluctuations at trieste. Physica A, 347: 695–703

Darby B J, Ritts B D (2002). Mesozoic contractional deformation in the middle of the Asian tectonic collage: the intraplate Western Ordos fold–thrust belt, China. Earth Planet Sci Lett, 205(1–2): 13–24

Fu J H, Li S X, Xu L M, Niu X B (2018). Paleo-sedimentary environmental restoration and its significance of Chang 7 Member of Triassic Yanchang Formation in Ordos Basin, NW China. Pet Explor Dev, 45(6): 998–1008

Ge X M, Fan Y R, Zhu X J, Deng S G, Wang Y (2014). A method to differentiate degree of volcanic reservoir fracture development using conventional well logging data—an application of kernel principal component analysis (KPCA) and multifractal detrended fluctuation analysis (MFDFA). IEEE J Sel Top Appl Earth Obs Remote Sens, 7 (12): 4972–4978

Hou G T (1994). Fractral geostatistics. Geology-geochemistry, 02: 68–70 (in Chinese)

Hou G T, Wang Y X, Hari K R (2010). The late Triassic and late Jurassic stress fields and tectonic transmission of North China craton. J Geodyn, 50(3–4): 318–324

Hu Z Q (2000). Application of *R*/*S* analysis in the evaluation of vertical reservoir heterogeneity and fracture development. Experimental Petroleum Geology, 22(5): 382–386 (in Chinese)

Hurst H E (1951). Long term storage capacity of reservoirs. Trans Am Soc Civ Eng, 116(12): 776–808

Ja'fari A, Kadkhodaie-Ilkhchi A, Sharghi Y, Ghanavati K (2012). Fracture density estimation from petrophysical log data using the adaptive neuro-fuzzy inference system. J Geophys Eng, 9(1): 105–114

Ju W, Niu X B, Feng S B, You Y, Xu K, Wang G, Xu H R (2020a). Present-day in-situ stress field within the Yanchang Formation tight oil reservoir of Ordos Basin, central China. J Petrol Sci Eng, 187: 106809

Ju W, Niu X B, Feng S B, You Y, Xu K, Wang G, Xu H R (2020b). Predicting the present-day in situ stress distribution within the Yanchang Formation Chang 7 shale oil reservoir of Ordos Basin, central China. Petrol Sci, 17(4): 912–924

Ju W, Sun W F, Hou G T (2015). Insights into the tectonic fractures in the Yanchang Formation interbedded sandstone-mudstone of the Ordos Basin based on core data and geomechanical models. Acta Geologica Sinica-English Edition, 89(6): 1986–1997

Lai J, Wang G W, Wang S, Cao J T, Li M, Pang X J, Han C, Fan X Q, Yang L, He Z B, Qin Z Q (2018). A review on the applications of image logs in structural analysis and sedimentary characterization. Mar Pet Geol, 95: 139–166

Li A, Ding W L, Luo K P, Xiao Z K, Wang R Y, Yin S, Deng M, He J H (2020). Application of *R*/*S* analysis in fracture identification of shale reservoir of the Lower Cambrian Niutitang Formation in northern Guizhou Province, South China. Geol J, 55(5): 4008–4020

Liu C Y, Zhao H G, Sun Y Z (2009). Tectonic background of Ordos Basin and its controlling role for basin evolution and energy mineral deposits. Energy Exploration and Exploitation, 27(1): 15–27

Liu L L, Zhao Z P, Li L, Chen W L, He Y A (2008). Application of the variable scale fractal technique in fracture prediction and reservoir

evaluation. Oil and Gas Geology, 29(1): 31–37 (in Chinese)

Lyu W Y, Zeng L B, Liu Z Q, Liu G P, Zu K W (2016). Fracture responses of conventional logs in tight-oil sandstones: a case study of the Upper Triassic Yanchang Formation in southwest Ordos Basin, China. AAPG Bull, 100(9): 1399–1417

Lyu W Y, Zeng L B, Zhang B J, Miao F B, Lyu P, Dong S Q (2017). Influence of natural fractures on gas accumulation in the Upper Triassic tight gas sandstones in the northwestern Sichuan Basin, China. Mar Pet Geol, 83: 60–72

Miranda J G V, Andrade R F S (1999). Rescaled range analysis of pluviometric records in northeast Brazil. Theor Appl Climatol, 63(1–2): 79–88

Pang J, North C P (1996). Fractals and their applicability in geological wireline log analysis. J Pet Geol, 19(3): 339–350

Rangarajan G, Sant D A (2004). Fractal dimensional analysis of Indian climatic dynamics. Chaos Solitons Fractals, 19(2): 285–291

Ritts B D, Hanson A D, Darby B J, Nanson L, Berry A (2004). Edimentary record of Triassic intraplate extension in North China: evidence from the nonmarine NW Ordos Basin, Helan Shan and Zhuozi Shan. Tectonophysics, 386(3–4): 177–202

Shi J X, Zeng L B, Zhao X Y, Zhang Y Z, Wang J P (2020). Characteristics of natural fractures in the upper Paleozoic coal bearing strata in the southern Qinshui Basin, China: implications for coalbed methane (CBM) development. Marine and Petroleum Geology, 113: UNSP10415

Su H, Lei Z D, Zhang D Q, Li J C, Zhang Z R, Ju B S, Li Z P (2017). Dynamic and static comprehensive prediction method of natural fractures in fractured oil reservoirs: a case study of Triassic Chang 63 reservoirs in Huaqing Oilfield, Ordos Basin, NW China. Pet Explor Dev, 44(6): 972–982

Tokhmechi B, Memarian H, Noubari H A, Moshiri B (2009). A novel approach proposed for fractured zone detection using petrophysical logs. J Geophys Eng, 6(4): 365–373

Wu S T, Zhu R K, Cui J G, Cui J W, Bai B, Zhang X X, Jin X, Zhu D S, Yao J L, You J C, Li X H (2015). Characteristics of lacustrine shale porosity evolution, Triassic Chang 7 Member, Ordos Basin, NW China. Petroleum Exploration and Development, 42(2): 185–195

Xiao Z K, Ding W L, Liu J S, Tian M Z, Yin S, Zhou X H, Gu Y (2019). A fracture identification method for low-permeability sandstone based on *R*/*S* analysis and the finite difference method: a case study from the Chang 6 reservoir in Huaqing Oilfield, Ordos Basin. J Petrol Sci Eng, 174: 1169–1178

Yang H, Liang X W, Niu X B, Feng S B, You Y (2017). Geological conditions for continental tight oil formation and the main controlling factors for the enrichment: a case of Chang 7 Member, Triassic Yanchang Formation, Ordos Basin, NW China. Petroleum Exploration and Development, 44(1): 11–19

Yang H, Niu X B, Xu L M, Feng S B, You Y, Liang X W, Wang F, Zhang D D (2016). Exploration potential of shale oil in Chang7 Member, Upper Triassic Yanchang Formation, Ordos Basin, NW China. Petroleum Exploration and Development, 43(4): 560–569

Zazoun R S (2013). Fracture density estimation from core and conventional well logs data using artificial neural networks: the Cambro-Ordovician reservoir of Mesdar oil field, Algeria. J Afr Earth Sci, 83: 55–73

Zeng L B, Li X Y (2009). Fractures in sandstone reservoirs with ultra-low permeability: a case study of the Upper Triassic Yanchang Formation in the Ordos Basin, China. AAPG Bull, 93(4): 461–477

Zeng L B, Liu H T (2010). Influence of fractures on the development of low-permeability sandstone reservoirs: a case study from the Taizhao district, Daqing Oilfield, China. J Petrol Sci Eng, 72(1–2): 120–127

Zeng L B, Lyu W Y, Li J, Zhu L F, Weng J Q, Yue F, Zu K W (2016). Natural fractures and their influence on shale gas enrichment in Sichuan Basin, China. J Nat Gas Sci Eng, 30: 1–9

Zeng L B, He Y H, Xiong W L (2010). Origin and Geological Significance of the Cross Fractures in the Upper Triassic Yanchang Formation, Ordos Basin, China. Energy Exploration & Exploitation, 28(2): 59–70

Zeng L B, Wang Z G, Xiao S R, Zhang G B (2009). The origin and geological significance of low dip-angle fractures in the thrust zones of the western basins of China. Acta Petrol Sin, 30(1): 56–60

Zhang X F, Pan B Z, Wang F, Han X (2011). A study of wavelet transforms applied for fracture identification and fracture density evaluation. Appl Geophys, 8(2): 164–169

Zhao J F, Chen X H, Zhang Q (2003). Application of grey association analysis in reservoir evaluation. Progress in Exploration Geophysics, 4: 282–286 (in Chinese)

Zhao W T, Hou G T (2017). Fracture prediction in the tight-oil reservoirs of the Triassic Yanchang Formation in the Ordos Basin, northern China. Petrol Sci, 14(1): 1–23

Zhao Z Y, Wang Y L, Liu G D, Sun X (2011). A rescaled range analysis on the characteristics of coal seam development in the eastern depression of the Liaohe Basin. Mining Science and Technology (China), 21(2): 223–227